

This discussion paper is/has been under review for the journal Atmospheric Chemistry and Physics (ACP). Please refer to the corresponding final paper in ACP if available.

Relationships between photosynthesis and formaldehyde as a probe of isoprene emission

Y. Zheng¹, N. Unger^{1,2}, M. P. Barkley³, and X. Yue²

¹Department of Geology and Geophysics, Yale University, New Haven, Connecticut 06511, USA

²School of Forestry and Environmental Studies, Yale University, New Haven, Connecticut 06511, USA

³EOS group, Department of Physics and Astronomy, University of Leicester, Leicester, UK

Received: 16 March 2015 – Accepted: 1 April 2015 – Published: 21 April 2015

Correspondence to: Y. Zheng (yiqi.zheng@yale.edu)

Published by Copernicus Publications on behalf of the European Geosciences Union.

ACPD

15, 11763–11797, 2015

Long-term isoprene variability

Y. Zheng et al.

Title Page

Abstract

Introduction

Conclusions

References

Tables

Figures

◀

▶

◀

▶

Back

Close

Full Screen / Esc

Printer-friendly Version

Interactive Discussion



Abstract

Atmospheric oxidation of isoprene emission from land plants affects radiative forcing of global climate change. There is an urgent need to understand the factors that control isoprene emission variability on large spatiotemporal scales but such direct observations of isoprene emission do not exist. Two readily available global-scale long-term observations hold information about surface isoprene activity: gross primary productivity (GPP) and tropospheric formaldehyde column variability (HCHOv). We analyze multi-year seasonal linear correlations between observed GPP and HCHOv. The observed GPP-HCHOv correlation patterns are used to evaluate a global Earth system model that embeds three alternative leaf-level isoprene emission algorithms. GPP and HCHOv are decoupled in the summertime southeast US ($r = -0.03$). In the Amazon, GPP-HCHOv are weakly correlated in March-April-May (MAM), correlated in June-July-August (JJA) and weakly anti-correlated in September-October-November (SON). Isoprene emission algorithms that include soil moisture dependence demonstrate greater skill in reproducing the observed interannual seasonal GPP-HCHOv correlations in the southeast US and the Amazon. In isoprene emission models that include soil moisture dependence, isoprene emission is correlated with photosynthesis and anti-correlated with HCHOv. In an isoprene emission model without soil moisture dependence, isoprene emission is anti-correlated with photosynthesis and correlated with HCHOv. Long-term monitoring of isoprene emission, soil moisture and meteorology is required in water-limited ecosystems to improve understanding of the factors controlling isoprene emission and its representation in global Earth system models.

1 Introduction

Isoprene emission, a by-product of photosynthesis, is fundamental in global chemistry-climate interactions. The global annual source strength is estimated at 0.5 PgC per year (Guenther et al., 2006), which is of comparable magnitude to the present day total

ACPD

15, 11763–11797, 2015

Long-term isoprene variability

Y. Zheng et al.

Title Page	
Abstract	Introduction
Conclusions	References
Tables	Figures
	
	
Back	Close
Full Screen / Esc	
Printer-friendly Version	
Interactive Discussion	



(anthropogenic and biogenic) annual source of methane (CH_4) (Kirschke et al., 2013), and the net carbon dioxide (CO_2) emission from land use change (Ciais et al., 2013). Isoprene emission rate depends upon ecosystem type, photosynthesis, temperature, and atmospheric CO_2 , and is therefore sensitive to changes in land cover and climate
5 (Monson et al., 2007). In contrast to CH_4 and CO_2 , isoprene is highly reactive in the atmosphere with a lifetime of around only half an hour in the boundary layer. The atmospheric photo-oxidation of isoprene regulates the global budgets and variability of the major short-lived climate pollutants: tropospheric ozone (O_3), CH_4 and secondary organic aerosol (Arneth et al., 2010; Carslaw et al., 2010). Large-scale perturbations to
10 isoprene emission influence global climate change (Scott et al., 2014; Unger, 2014a). In Earth's history, plant isoprene emission is recognized as an important terrestrial biogeochemical feedback that influences the global climate sensitivity (Beerling et al., 2007, 2011; Unger and Yue, 2014). Emerging research begins to quantify isoprene's role as an anthropogenic climate forcing mechanism (Heald and Spracklen, 2015;
15 Unger, 2014b). While short-term weather-related fluctuations in isoprene emission in the temperate zone are well understood (Guenther et al., 1995, 1991), many open questions remain as to the long-term factors controlling isoprene emission. A complete understanding of isoprene emission on large spatiotemporal scales is imperative to allow reliable projections of future air quality and global climate change, and to discern
20 quantitatively the real-world effectiveness of mitigation strategies involving the short-lived climate pollutants.

Two readily available global observations do hold information about isoprene emission variability: (i) gross primary productivity (GPP) and (ii) satellite tropospheric formaldehyde (HCHO) columns. GPP is the total amount of CO_2 removed from the atmosphere by plant photosynthesis. Isotopic labeling studies have shown that 70–90 % of isoprene production is directly linked to photosynthesis that provides energy and precursors for isoprene biosynthesis in the chloroplast (Affek and Yakir, 2003; Delwiche and Sharkey, 1993; Karl et al., 2002). Precipitation controls photosynthesis in more than 40 % of vegetated land (Beer et al., 2010). HCHO is a high-yield product
25

Long-term isoprene variability

Y. Zheng et al.

[Title Page](#)

[Abstract](#)

[Introduction](#)

[Conclusions](#)

[References](#)

[Tables](#)

[Figures](#)

[|◀](#)

[▶|](#)

[◀](#)

[▶](#)

[Back](#)

[Close](#)

[Full Screen / Esc](#)

[Printer-friendly Version](#)

[Interactive Discussion](#)



of isoprene oxidation and has a lifetime of only a few hours against photolysis and oxidation by the hydroxyl radical during the day. Since isoprene emission frequently dominates the volatile organic compound (VOC) budget over continental land, HCHO columns have been used as a direct proxy for inferring isoprene emissions (Barkley et al., 2008, 2013; Fu et al., 2007; Millet et al., 2008; Palmer et al., 2003, 2006).

Neither GPP nor HCHO columns offer a perfect indicator of isoprene emission variability. In the case of GPP, incomplete coupling between isoprene emission and photosynthesis occurs due to the different temperature optima of the processes, response to short-term drought and elevated atmospheric CO₂, and onset time in the deciduous biome (Harrison et al., 2013). The optimal temperature for photosynthesis is around 25 °C while isoprene emission has a higher thermal optimum of 35–40 °C. In the case of HCHO columns, limitations in use as a direct proxy for isoprene include: (1) uncertainties associated with the HCHO vertical column retrieval (Barkley et al., 2012; Hewson et al., 2013), (2) distinguishing the component of the HCHO column produced solely from isoprene oxidation, and (3) uncertainties in isoprene oxidation chemistry.

Isoprene provides an intrinsic linkage between GPP and atmospheric HCHO. A recent study found a strong intra-seasonal correlation between satellite HCHO columns and canopy temperature but a weak correlation or even anti-correlation with GPP in 22 regions selected to minimize interference from fires (Foster et al., 2014). In that study, HCHO columns were assumed to be a direct proxy for surface isoprene emission. Soil moisture availability was not explicitly considered as a driving variable even though water availability and canopy temperature are tightly coupled through stomatal conductance and the canopy energy balance. Accounting for soil moisture dependence of isoprene emission decreases the global source strength by 25–30 % (Muller et al., 2008; Unger et al., 2013).

Here, we investigate the multi-year (2005–2011) seasonal relationships between global observational datasets of FLUXNET-derived GPP and fire-screened satellite HCHO columns as a probe of isoprene emission on longer seasonal to interannual temporal scales. We assume that observed GPP and HCHO columns hold quantita-

Long-term isoprene variability

Y. Zheng et al.

[Title Page](#)

[Abstract](#)

[Introduction](#)

[Conclusions](#)

[References](#)

[Tables](#)

[Figures](#)

[|◀](#)

[▶|](#)

[◀](#)

[▶](#)

[Back](#)

[Close](#)

[Full Screen / Esc](#)

[Printer-friendly Version](#)

[Interactive Discussion](#)



2 Methods

2.1 Observational and reanalysis datasets

In this study we apply datasets of observational GPP, satellite-based tropospheric HCHO columns and meteorology reanalysis. The monthly-mean global GPP dataset is generated using data orientated diagnostic upscaling of site-level derived GPP from FLUXNET (Beer et al., 2010; Bonan et al., 2011; Jung et al., 2011) and is available for years 1982–2011 with native resolution of $0.5^\circ \times 0.5^\circ$ latitude by longitude.

The fire-screened monthly mean tropospheric HCHO vertical columns are retrieved by the Ozone Monitoring Instrument (OMI) over 2005–2013. We compute the fire-screened tropospheric HCHO vertical columns from retrieved slant columns provided in the official NASA OMI product (González Abad et al., 2015), in a three step process. First, we apply our own reference sector correction to normalize the HCHO columns, on a daily basis. This is a standard technique used in many studies to remove retrieval biases (e.g., Barkley et al., 2013; González Abad et al., 2015; Marais et al., 2012). Here we compute the median OMI slant columns (Ω_{SM}) in 1° latitude bins over the remote Pacific Ocean ($140\text{--}160^\circ\text{W}$), and subtract this latitudinal bias from all retrieved slant columns (Ω_{S}). We then re-normalize the vertical columns (Ω_{V}) by adding a model

Title Page	
Abstract	Introduction
Conclusions	References
Tables	Figures
Back	Close
Full Screen / Esc	
Printer-friendly Version	
Interactive Discussion	



HCHO latitudinal background (Ω_{VB}), provided by the NASA ModelE2-YIBs simulation (described in Sect. 2.2), as follows:

$$\Omega_V = \frac{\Omega_S - \Omega_{SM}}{AMF} + \Omega_{VB} \quad (1)$$

where AMF is the air mass factor, defined as the ratio of the slant and vertical columns.

- 5 Second, we generate AMF look-up tables using monthly averaged HCHO profiles from the global earth system model NASA ModelE2-YIBs (three sub-versions, as described in Sect. 2.2), appropriate to the OMI's overpass time. The AMF calculation is the same as that described in Barkley et al. (2013), with the exception that no aerosol correction is applied as model aerosol optical depth (AOD) profiles were not available. Third, we
10 then apply the AMFs to the corrected slant columns, using Eq. (1), and average the resulting vertical columns onto a generic global $0.5^\circ \times 0.5^\circ$ latitude–longitude grid. We additionally filter the OMI data, excluding scenes with $\geq 40\%$ cloud cover and that do not meet standard quality checks (González Abad et al., 2015); observations affected by the documented OMI row anomaly are also discarded. To remove biomass burning
15 contamination from the data, we adopt the method devised by Barkley et al. (2013) which excludes fire-affected scenes using Advanced Along-Track Scanning Radiometer (AATSR) and Moderate Resolution Imaging Spectroradiometer (MODIS) active burning detections. Individual observations are discarded if a fire occurs in the 0.5° grid-cell in which it falls, or those immediately adjacent (within ± 2 grid-cells), of both
20 the current or preceding day. The uncertainties on the gridded OMI vertical columns are estimated at 5–20 % (Barkley et al., 2013). To ensure consistency in our satellite-model comparisons, the reference correction and AMFs are recomputed using HCHO profiles from the appropriate model simulation. In our subsequent analysis, we use the HCHO column variability (HCHO_v), which is defined as the anomaly between local and
25 zonal mean of the gridded fire-screened HCHO tropospheric column concentrations for each month, to explore its climatic covariance and relationship with GPP, and compare against the NASA ModelE2-YIBs output.

Title Page	
Abstract	Introduction
Conclusions	References
Tables	Figures
	
	
Back	Close
Full Screen / Esc	
Printer-friendly Version	
Interactive Discussion	



Title Page

Abstract

Introduction

Conclusions

References

Tables

Figures

◀

▶

◀

▶

Back

Close

Full Screen / Esc

Printer-friendly Version

Interactive Discussion



We use monthly-mean meteorological variables, including surface temperature (T_s), downward short wave radiation (SW), photosynthetically active radiation (PAR), and precipitation (P), from the NASA Modern Era Retrospective-Analysis for Research and Applications (MERRA) (Rienecker et al., 2011). The spatial resolution of the MERRA data is $0.5^\circ \times 0.667^\circ$ latitude by longitude and the temporal availability is 1979 to present. The analyses in this study apply data from the observational overlap period (2005–2011).

All of the monthly average observational datasets are linearly interpolated to $2.0^\circ \times 2.5^\circ$ latitude by longitude spatial resolution.

10 2.2 Global Earth system model (NASA ModelE2-YIBs)

This study applies the NASA GISS ModelE2 global chemistry-climate model at $2^\circ \times 2.5^\circ$ latitude by longitude horizontal resolution with 40-vertical layers extending to 0.1 hPa (Schmidt et al., 2014). The Yale Interactive Terrestrial Biosphere Model (YIBs) is embedded inside NASA ModelE2 in a framework known as NASA ModelE2-YIBs. The global climate model provides the meteorological drivers for the vegetation biophysics. The land-surface hydrology submodel provides soil characteristics to the vegetation physiology in each grid cell. The model framework fully integrates the land biosphere-oxidant-aerosol system such that these components interact with each other and with the physics of the climate model at the 30 min integration time step. The atmospheric composition model has been well tested against observations and compared with other models e.g. (Koch et al., 2010; Myhre et al., 2013; Shindell et al., 2013a, b; Stevenson et al., 2013).

The vegetation is described using eight plant functional types (PFTs): tundra, C3 and C4 grassland, shrub, deciduous, tropical rainforest, evergreen, and crop. Present-day vegetation cover fractions are derived from Moderate Resolution Imaging Spectroradiometer (MODIS) satellite data as used in the Community Land Model and converted to the eight PFTs here (Lawrence and Chase, 2007). PFT-specific leaf area index (LAI)

[Title Page](#)[Abstract](#)[Introduction](#)[Conclusions](#)[References](#)[Tables](#)[Figures](#)[|◀](#)[▶|](#)[◀](#)[▶](#)[Back](#)[Close](#)[Full Screen / Esc](#)[Printer-friendly Version](#)[Interactive Discussion](#)

is derived from Advanced Very High Resolution Radiometer (AVHRR) satellite data and linearly interpolated into daily values (Lawrence and Chase, 2007).

The canopy biophysical fluxes are computed using the well established Michealis–Menten leaf model of photosynthesis (von Caemmerer and Farquhar, 1981; Farquhar et al., 1980) and the stomatal conductance model of Ball and Berry (Collatz et al., 1991). The model vertically stratifies each canopy into an adaptive number of layers (typically 2–16) that distinguish LAI profiles for sunlit and shaded leaves (Friend and Kiang, 2005).

2.2.1 Isoprene emission algorithms

NASA ModelE2-YIBs incorporates two conceptually different leaf-level isoprene emission algorithms that are embedded within the exact same host simulation framework: (1) Y-PS: isoprene emission is calculated as a function of electron transport-limited photosynthesis, intercellular and atmospheric CO₂ and canopy temperature (Unger et al., 2013) and (2) Y-MEGAN: isoprene emission is calculated using empirical functions of canopy temperature and light commonly applied in the Model of Emissions of Gases and Aerosols from Nature (MEGAN) (Guenther et al., 1995). MEGAN is the most widely used system for estimating isoprene emissions from terrestrial ecosystems (Guenther et al., 2012). We test a third isoprene emission algorithm identical to Y-MEGAN but with an additional empirical multiplier to account for soil moisture availability (Y-MEGAN-SM).

In Y-PS, leaf-level isoprene emission is modeled as follows:

$$I_{\text{emis}} = \varepsilon \cdot J_e \cdot \delta \cdot \tau \quad (2)$$

where ε is the PFT-specific isoprene emission potential in units of fraction of electrons available for isoprene synthesis. J_e is the electron transport limited photosynthesis rate in units of $\mu\text{mol m}^{-2} [\text{leaf}] \text{s}^{-1}$. J_e is a linear function of the incident photosynthetically

active radiation (PAR) and the internal leaf CO₂ concentration (C_i):

$$J_e = a_{leaf} \cdot PAR \cdot \alpha_{qe} \cdot \frac{C_i - \Gamma^*}{C_i + 2\Gamma^*} \quad (3)$$

where a_{leaf} is the leaf specific light absorptance, α_{qe} is the intrinsic quantum efficiency for photosynthetic CO₂ uptake in photosystem II (a product of the fraction of absorbed

- 5 light that reaches photosystem II and the CO₂ per absorbed photon), and Γ^* is the CO₂ concentration compensation point in the absence of non-photorespiratory respiration (Collatz et al., 1991).

The δ term in Eq. (2) translates the electron flux into isoprene equivalents given by Eq. (4) detailed in (Niinemets et al., 1999; Pacifico et al., 2011):

$$10 \quad \delta = \frac{C_i - \Gamma^*}{6(4.67C_i + 9.33\Gamma^*)} \quad (4)$$

The temperature relationship (τ) in the algorithm accounts for the difference in temperature optimum between photosynthesis and isoprene synthase:

$$\tau = \exp [0.1(T - T_{ref})] \quad (5)$$

where T is leaf temperature in °C and T_{ref} is the leaf temperature under standard conditions (30 °C).

In Y-MEGAN, leaf-level isoprene emission is modeled following:

$$I_{emis} = E \cdot C_T \cdot C_L \quad (6)$$

where E is the PFT-specific isoprene emission potential in units of μmol C m⁻² s⁻¹:

$$15 \quad C_T = \frac{\exp \frac{C_{T1}(T_K - T_{Ks})}{RT_{Ks}T_K}}{1 + \exp \frac{C_{T2}(T_K - T_M)}{RT_{Ks}T_K}} \quad (7)$$

Title Page

Abstract

Introduction

Conclusions

References

Tables

Figures

◀

▶

Back

Close

Full Screen / Esc

Printer-friendly Version

Interactive Discussion



and:

$$C_L = \frac{\alpha C_{L1} \text{PAR}}{\sqrt{1 + \alpha^2(\text{PAR})^2}} \quad (8)$$

T_K is the leaf temperature in Kelvin, T_{Ks} is the leaf temperature at standard conditions (= 303 K), R is the ideal gas constant (= 8.314 JK⁻¹ mol⁻¹); C_{T1} (= 95 000 J mol⁻¹),

5 C_{T2} (= 230 000 J mol⁻¹), T_M (= 314 K), α (= 0.0027) and C_{L1} (= 1.066) are empirical coefficients.

Y-PS and Y-MEGAN use identical PFT-specific isoprene emission potentials converted to the relevant units for ε (unitless) and E ($\mu\text{mol C m}^{-2} \text{s}^{-1}$), presented here in units of $\mu\text{g C g}^{-1} \text{h}^{-1}$: tundra = 0, C3 grassland = 16, C4 grassland = 0, shrub = 16, deciduous = 45, tropical rainforest = 24, evergreen = 8, and crop = 0 (Guenther, 2007; Lathiere et al., 2006). An additional multiplier to account for the long-term atmospheric CO₂-sensitivity of isoprene emission is applied to both isoprene models that is normalized to 1.0 for the present-day atmospheric CO₂ levels used in this study (Arneth et al., 2007).

15 Y-MEGAN-SM is identical to Y-MEGAN but includes an additional multiplier to account for soil moisture availability following the approach used in the coupled photosynthesis-stomatal conductance vegetation biophysics submodel. The multiplier value is between 0 and 1 and reflects the relationship between soil water amount and the extent of stomatal closure ranging from no water stress to the soil moisture stress onset point (s^*) through to the wilting point (s_{wilt}) (Porporato et al., 2001). The multiplier value is reduced linearly between the PFT-specific values of s^* and s_{wilt} based on the climate model's soil water volumetric saturation in six soil layers. Values of s^* and s_{wilt} are documented in Unger et al. (2013).

20 The leaf-level isoprene emissions in each isoprene scheme are upscaled to the canopy level using the YIBs canopy vertical stratification and integration scheme (Unger et al., 2013). The canopy level isoprene fluxes are passed to the model's atmosphere through the land-surface scheme on the 30 min integration time step of the

[Title Page](#)

[Abstract](#)

[Introduction](#)

[Conclusions](#)

[References](#)

[Tables](#)

[Figures](#)

[|◀](#)

[▶|](#)

[◀](#)

[▶](#)

[Back](#)

[Close](#)

[Full Screen / Esc](#)

[Printer-friendly Version](#)

[Interactive Discussion](#)



global climate model. Thus, the three isoprene emission algorithms “see” the exact same PFT-specific isoprene emission potentials (basal rates), vegetation input data and meteorology, and apply the exact same upscaling from leaf to canopy. In Y-PS, the light dependence occurs through the linkage to photosynthesis; in Y-MEGAN and

5 Y-MEGAN-SM, isoprene emission is directly related to PAR. All three models are directly linked to canopy temperature. In Y-PS, soil moisture dependence occurs through the linkage to photosynthesis; Y-MEGAN has no direct soil moisture dependence but captures indirect effects through canopy temperature changes; and Y-MEGAN-SM has soil moisture dependence through the additional empirical multiplier.

10 2.2.2 Simulations

We perform three NASA ModelE2-YIBs simulations representative of present day (2000s) climatology for each of the isoprene emission schemes (Y-PS; Y-MEGAN; Y-MEGAN-SM). Decadal average (1996–2005) monthly-varying sea surface temperature and sea ice climatology from the HadSST2 dataset provide the physical climatic boundary conditions for the simulations (Rayner et al., 2006). The present day anthropogenic trace gas and aerosol emissions are prescribed to year 2000 values from the inventory developed for IPCC AR5 (Lamarque et al., 2010). Atmospheric levels of long-lived greenhouse gases are prescribed to $\text{CO}_2 = 370 \text{ ppmv}$, $\text{CH}_4 = 1733 \text{ ppbv}$ in Southern Hemisphere (SH) and 1814 ppbv in Northern Hemisphere (NH), $\text{N}_2\text{O} = 316 \text{ ppbv}$. Integrations of eleven model years are completed for all control and sensitivity simulations; the first two years of the simulations are discarded as spin-up and the remaining nine years are used for analyses.

25 3 Results

Using the exact same vegetation input data, meteorology and PFT-specific basal rates, the three isoprene algorithms give substantially different annual global iso-

Title Page

Abstract

Introduction

Conclusions

References

Tables

Figures

◀

▶

◀

▶

Back

Close

Full Screen / Esc

Printer-friendly Version

Interactive Discussion



prene emission strengths: 382 Tg C year⁻¹ for Y-PS, 452 Tg C year⁻¹ for Y-MEGAN and 263 Tg C year⁻¹ for Y-MEGAN-SM. As shown in Fig. 1 (left column), isoprene emission in Y-MEGAN is lower in NH mid-latitudes than Y-PS, and is stronger in the tropics. Y-MEGAN-SM has lower isoprene flux than Y-MEGAN, especially in the dry subtropics in South America, Africa and Australia. Yet, the three OMI HCHO column datasets that use different AMFs for the three isoprene models show similar distribution (Fig. 1, right column). Further analysis of OMI HCHO column datasets, including the multiple linear regression (MLR) of HCHOv with meteorological variables in Sect. 3.1 and the observation correlation between GPP and HCHOv in Sect. 3.2, show no difference among the three HCHO datasets. Therefore, in the following analyses, results shown are based on OMI-HCHO processed using Y-PS AMFs.

3.1 Meteorological drivers of GPP and HCHOv

The regionally averaged meteorological variables T_s , PAR, SW and P for the period 2005–2011 from MERRA reanalysis and the climate model NASA ModelE2-YIBs are summarized in Table 1. In MERRA, the average T_s values for March-April-May (MAM), June-July-August (JJA) and September-October-November (SON) in key regions are (in °C): 18.0±0.8, 26.8±0.5, 18.6±0.8 (southeast US); 23.5±0.5, 23.7±0.4, 25.3±0.6 (Amazon). Seasonal average T_s in southeast US in JJA and in the Amazon in SON slightly exceed the photosynthetic thermal optimum (25 °C). No vegetated region on the planet has a seasonal average T_s that exceeds the thermal optimum of isoprene emission (35–40 °C).

Figure 2 shows the multiple linear regression (MLR) results for monthly average GPP (1982–2011) and HCHOv (2005–2013) in three seasons (MAM, JJA, SON) against T_s , PAR (SW for HCHOv), and P . The computed standardized partial regression coefficients (β -coefficients) represent the rate of change in the dependent variable for a unit change in the independent variable with all other independent variables held constant. The coefficients have been standardized in units of SD, thus they can be directly

Long-term isoprene variability

Y. Zheng et al.

[Title Page](#)

[Abstract](#)

[Introduction](#)

[Conclusions](#)

[References](#)

[Tables](#)

[Figures](#)

[◀](#)

[▶](#)

[◀](#)

[▶](#)

[Back](#)

[Close](#)

[Full Screen / Esc](#)

[Printer-friendly Version](#)

[Interactive Discussion](#)



compared with each other to determine the relative importance of the different driving variables. The standardized partial regression coefficients of GPP and HCHOv associated with T_s , PAR (SW for HCHOv) and P are denoted by $\text{GPP}_\beta T_s$, $\text{GPP}_\beta \text{PAR}$, $\text{GPP}_\beta P$ and $\text{HCHOv}_\beta T_s$, $\text{HCHOv}_\beta \text{SW}$, $\text{HCHOv}_\beta P$. GPP β -coefficients are statistically significant ($p < 0.05$) over most vegetated regions of the planet. HCHOv β -coefficients are not significant to 95 % confidence level anywhere on the planet. Several reasons are responsible for the difference in significance: the GPP dataset has a longer record (1982–2011) than the HCHO dataset (2005–2013); GPP is a derived product from upscaling of site-level measurements, while remote-sensed HCHO columns are relatively noisy due to the satellite retrieval method (Palmer et al., 2001; De Smedt et al., 2008); perhaps more importantly, unlike GPP which has a simple near-parabolic relationship with T_s , HCHO dependence on T_s is more complex. For instance, increasing T_s promotes isoprene emission and oxidation to HCHO, but also accelerates the chemical destruction of HCHO (see Supplement and Fig. S1).

The regionally averaged β -coefficients over southeast US (31 to 35° N; –94 to –79° E) and the Amazon (–15 to 3° N; –76 to –54° E) are summarized in Table 2. GPP is strongly positively related to T_s in the NH springtime and summertime high-latitudes (Fig. 2). In NH mid-latitudes in summer, where T_s values approach and/or exceed the photosynthetic thermal optimum, sensitivity to T_s decreases dramatically. In the southeast US, $\text{GPP}_\beta T_s$ drops from 0.58 in spring to 0.03 in summer. In NH subtropical and semi-arid regions, there is a marked anticorrelation with T_s in the NH summer ($\text{GPP}_\beta T_s < -0.3$). In contrast, HCHOv is generally positively correlated with T_s across all continents and seasons. The averaged $\text{HCHOv}_\beta T_s$ values in the southeast US are 0.36, 0.31 and 0.53 in MAM, JJA and SON. In the Amazon, the temperature dependence of both GPP and HCHOv are positive but weak.

GPP has a strong positive relationship with PAR in NH mid-latitudes (especially in SON) and in tropical continents in all seasons (Fig. 2). The spatial pattern of HCHOv dependence on SW is extremely patchy because HCHO can be both formed and destroyed by photolysis. In the southeast US, $\text{GPP}_\beta \text{PAR}$ are 0.44, 0.41, 0.51 in MAM,

Long-term isoprene variability

Y. Zheng et al.

[Title Page](#)

[Abstract](#)

[Introduction](#)

[Conclusions](#)

[References](#)

[Tables](#)

[Figures](#)

[◀](#)

[▶](#)

[◀](#)

[▶](#)

[Back](#)

[Close](#)

[Full Screen / Esc](#)

[Printer-friendly Version](#)

[Interactive Discussion](#)



JJA and SON, whereas HCHOv $_{\beta}$ _SW are –0.02, 0.16 and –0.18; the Amazon also shows relatively strong positive light dependence of GPP (0.46, 0.57, 0.17). In the Amazon, HCHOv displays no apparent relationship with SW in MAM and SON but a positive relationship in JJA (0.00, 0.31, 0.01).

- 5 The relationship between GPP and precipitation is always positive over heavily vegetated regions. GPP $_{\beta}$ _P values tend to be weaker than GPP $_{\beta}$ T_s and GPP $_{\beta}$ PAR values in the NH middle to high latitudes, but much stronger in the tropical rainforest regions in MAM and SON. In the tropics, precipitation stimulates GPP significantly in MAM and SON (GPP $_{\beta}$ _P = 0.70 in MAM and 0.50 in SON). In contrast, there is no
10 detectable relationship between precipitation and HCHOv in this region in MAM and JJA, but a strong anti-correlation in SON. Precipitation dampens local photochemistry by removing reactive carbon and nitrogen compounds. Although wet deposition is not a major sink for HCHO due to the relatively low Henry's Law coefficient, previous studies have found an anti-correlation with precipitation in highly polluted regions (Báez
15 et al., 1993).

3.2 Observed GPP-HCHOv correlation

- Figure 3 shows the Pearson's correlation coefficient (r) between monthly mean observational GPP and HCHOv for each season calculated using the 2005–2011 data. We show results where FLUXNET-GPP is greater than $0.01 \text{ g[C] m}^{-2} \text{ day}^{-1}$ for the latitude range -50° S to $+50^{\circ}$ N (except in boreal summer) because the satellite HCHO columns have known large biases in high-latitudes under limited-light conditions (De Smedt et al., 2008; Wittrock et al., 1997). The observed GPP-HCHOv correlation varies
20 strongly with latitude and season. Regionally averaged seasonal correlation values for the southeast US and the Amazon are shown in Table 3. The southeast US shows a significant GPP-HCHOv coupling in transition seasons ($r = 0.24$ in boreal spring and
25 $r = 0.25$ in fall, $p < 0.05$), which is likely driven by their covariance with temperature. In boreal summer, this positive correlation signal moves northward to NH high-latitudes where boreal forests emit terpenoids. GPP and HCHOv in the summertime southeast

Long-term isoprene variability

Y. Zheng et al.

[Title Page](#)

[Abstract](#)

[Introduction](#)

[Conclusions](#)

[References](#)

[Tables](#)

[Figures](#)

[|◀](#)

[▶|](#)

[◀](#)

[▶](#)

[Back](#)

[Close](#)

[Full Screen / Esc](#)

[Printer-friendly Version](#)

[Interactive Discussion](#)



US are almost decoupled with a very weak anti-correlation signal ($r = -0.03$). Similar decoupling or weak anti-correlation occurs in the tropics all the year round except in the Amazon in JJA ($r = 0.33$).

3.3 Model GPP-HCHOv correlation

- We examine the simulated GPP-HCHOv correlations in NASA ModelE2-YIBs for the three isoprene emission algorithms: Y-PS, Y-MEGAN and Y-MEGAN-SM. Overall, the simulated GPP-HCHOv r values are stronger than the observed values everywhere on the planet. Generally, overestimates of GPP-HCHOv r values in the models may be due to over-simplified parameterizations of biogeochemical processes and photochemical oxidation mechanisms, missing, possibly important but highly uncertain, processes in the models, for instance nutrient availability, and the use of generic PFT-specific isoprene emission potentials. The three models successfully reproduce the GPP-HCHOv correlation pattern in the NH temperate spring and fall transition seasons that is likely driven by covariance with temperature (Fig. 4a). They broadly capture the observed GPP-HCHOv spatial patterns in the tropics in MAM and SON, but not in JJA. The models' overestimate of the positive correlation in southeast US in spring and fall may be because the algorithms do not include the delayed onset in spring or earlier shutdown of isoprene emission before senescence. Regionally averaged model correlation results for the southeast US and the Amazon are compared with the observational results in Table 3. In contrast to the observed GPP-HCHOv decoupling (no correlation) in the summertime southeast US, the models simulate anti-correlation but to different extents: $r = -0.19$ (Y-PS); $r = -0.62$ (Y-MEGAN); $r = -0.37$ (Y-MEGAN-SM). In the Amazon, Y-PS and Y-MEGAN-SM reproduce the observed GPP-HCHOv correlations in MAM and SON but are unable to reproduce the observed strong positive correlation there in JJA. Y-MEGAN fails to reproduce the seasonal observed GPP-HCHOv correlations in the Amazon; for this model, GPP-HCHOv are anti-correlated in JJA ($r = -0.08$) where observed GPP-HCHOv $r = 0.33$; and strongly anti-correlated in SON ($r = -0.51$) where

Title Page	
Abstract	Introduction
Conclusions	References
Tables	Figures
	
	
Back	Close
Full Screen / Esc	
Printer-friendly Version	
Interactive Discussion	



observed GPP-HCHOv $r = -0.09$). In the Amazon in JJA, GPP is strongly related to PAR; similarly HCHOv is related to SW (Sect. 3.1).

Poor performance of all models in Amazon JJA may be due to the global climate model's simulation of meteorology. Simulated T_s ($26.4 \pm 0.3^\circ\text{C}$) in the Amazon JJA is 2~
5 3 °C higher than the MERRA T_s ($23.7 \pm 0.4^\circ\text{C}$) and exceeds the GPP thermal optimum
(25°C). This temperature overestimation likely contributes to the non-real decoupling
or weak anti-correlation between GPP and HCHOv in the three models.

To probe the underlying causes of the GPP-HCHOv relationships, we examine the
model correlations between isoprene emission (ISOPe) and GPP, and between ISOPe
10 and HCHOv shown in Fig. 4b and c. Regionally averaged values for the southeast US
and the Amazon are compared in Table 3. It is apparent that the GPP-HCHOv rela-
tionships are driven by different underlying causes contingent upon whether the iso-
15 prene emission algorithm includes soil moisture dependence. Focusing on southeast
US, Y-PS indicates linear coupling between GPP and ISOPe ($r = 0.94 \pm 0.07$), and only
a weak or even anti-correlation between ISOPe and HCHOv in summertime south-
20 east US ($r = -0.03 \pm 0.31$). In contrast, Y-MEGAN indicates strong coupling between
ISOPe and HCHOv ($r = 0.73 \pm 0.09$), but anti-correlation between GPP and ISOPe in
the summer ($r = -0.39 \pm 0.23$).

In Y-PS, anti-correlation between GPP and HCHOv is determined by the anti-
20 correlation between ISOPe and HCHOv. On interannual seasonal time scales, precipi-
tation positively stimulates GPP but has no direct impact on HCHOv, which is predom-
inantly controlled by temperature (see Supplement). Photochemical production and
loss of HCHO strongly depend on temperature and light independent of isoprene emis-
25 sion (e.g. Seinfeld and Pandis, 2006; Fig. 2b; Fig. S1b). Furthermore, HCHOv may be
influenced by emission and oxidation of non-isoprene VOCs. In Y-MEGAN, the anti-
correlation between GPP and ISOPe drives the GPP-HCHOv anti-correlation in this
model under conditions when the thermal optimum of photosynthesis has been ex-
ceeded. Y-MEGAN-SM displays more Y-PS-like behavior, a correlation between GPP
and ISOPe, but anti-correlation between ISOPe and HCHOv in summertime southeast

Title Page

Abstract

Introduction

Conclusions

References

Tables

Figures

|◀

▶|

◀

▶

Back

Close

Full Screen / Esc

Printer-friendly Version

Interactive Discussion



Title Page

Abstract

Introduction

Conclusions

References

Tables

Figures

◀

▶

◀

▶

Back

Close

Full Screen / Esc

Printer-friendly Version

Interactive Discussion



US and in MAM and SON in the Amazon. This result suggests the importance of water availability as a control on the photosynthesis-ISOPe-HCHO system: all the three processes are strongly influenced by temperature, but the dependence on soil moisture determines the summertime covariance of photosynthesis and isoprene variability,

5 which can over-ride their anti-correlation due to different thermal optima. The relative lack of sensitivity of HCHOv to water availability and precipitation leads to weaker correlation or even anti-correlation behavior between ISOPe and HCHOv.

4 Discussion and conclusions

We find that all three models reproduce the observed NH mid-latitude GPP-HCHOv

10 correlation in spring and fall, but predict anti-correlation in summer when the observations suggest decoupling. The underlying causes for the predicted relationships are isoprene-algorithm-dependent. In the isoprene algorithms that account for soil moisture dependence (Y-PS and Y-MEGAN-SM), interannual seasonal isoprene emission variability is tightly linked to photosynthesis but anti-correlated with HCHO variability; 15 the dependence on soil moisture determines the summertime covariance of isoprene emission and photosynthesis, which override their opposite response to high temperature. While in Y-MEGAN, isoprene emission is anti-correlated with photosynthesis at high temperatures due to their different thermal optima, and is strongly correlated with HCHO variability.

20 This research raises more questions about long-term isoprene emission variability than it answers. Ground truthing of the findings is impeded by the lack of long-term isoprene emission flux tower and meteorology measurements in water-limited ecosystems. However, our results do suggest that water availability may be an important driver of vegetation-chemistry-climate interactions under future global change. A corollary is 25 that on longer time scales (seasonal, annual, decadal), GPP may be a more reliable indicator of surface isoprene emission than HCHOv. The soil moisture dependence of isoprene emission warrants further research. Long-term direct measurements of

Long-term isoprene variability

Y. Zheng et al.

[Title Page](#)

[Abstract](#)

[Introduction](#)

[Conclusions](#)

[References](#)

[Tables](#)

[Figures](#)

[|◀](#)

[▶|](#)

[◀](#)

[▶](#)

[Back](#)

[Close](#)

[Full Screen / Esc](#)

[Printer-friendly Version](#)

[Interactive Discussion](#)



isoprene emission co-located with meteorological monitoring are essential to provide more information on the extent of water dependence of isoprene. Global Earth system models used to study long-term changes in isoprene emission should include soil moisture dependence. Currently, soil moisture is poorly represented in land-surface and climate models (Koster et al., 2009). The recent launch of the NASA Soil Moisture Active Passive instrument will produce global maps of soil moisture and was designed to help improve understanding of carbon and water cycles. Inadvertently, this dataset may also help improve understanding of isoprene emission and atmospheric chemistry.

**The Supplement related to this article is available online at
doi:10.5194/acpd-15-11763-2015-supplement.**

Author contributions. N. Unger and Y. Zheng designed this study and developed the model code. Y. Zheng performed the simulations and analysis. M. P. Barkley processed the satellite-based formaldehyde data. X. Yue contributed to the model development. Y. Zheng, N. Unger and M. P. Barkley wrote the manuscript.

Acknowledgements. Funding support for this research is provided by the NASA Atmospheric Composition Campaign Data Analysis and Modeling Program. This project was supported in part by the facilities and staff of the Yale University Faculty of Arts and Sciences High Performance Computing Center.

References

- 20 Affek, H. P. and Yakir, D.: Natural abundance carbon isotope composition of isoprene reflects incomplete coupling between isoprene synthesis and photosynthetic carbon flow, *Plant Physiol.*, 131, 1727–1736, doi:10.1104/pp.102.012294, 2003.
- Arneth, A., Niinemets, Ü., Pressley, S., Bäck, J., Hari, P., Karl, T., Noe, S., Prentice, I. C., Serça, D., Hickler, T., Wolf, A., and Smith, B.: Process-based estimates of terrestrial ecosystem isoprene emissions: incorporating the effects of a direct CO₂-isoprene interaction, *Atmos. Chem. Phys.*, 7, 31–53, doi:10.5194/acp-7-31-2007, 2007.

Long-term isoprene variability

Y. Zheng et al.

[Title Page](#)

[Abstract](#)

[Introduction](#)

[Conclusions](#)

[References](#)

[Tables](#)

[Figures](#)

[|◀](#)

[▶|](#)

[◀](#)

[▶](#)

[Back](#)

[Close](#)

[Full Screen / Esc](#)

[Printer-friendly Version](#)

[Interactive Discussion](#)



Arneth, A., Sitch, S., Bondeau, A., Butterbach-Bahl, K., Foster, P., Gedney, N., de Noblet-Ducoudré, N., Prentice, I. C., Sanderson, M., Thonicke, K., Wania, R., and Zaehle, S.: From biota to chemistry and climate: towards a comprehensive description of trace gas exchange between the biosphere and atmosphere, *Biogeosciences*, 7, 121–149, doi:10.5194/bg-7-121-2010, 2010.

5 Baez, A. P., Padilla, H. G., and Belmont, R. D.: Scavenging of atmospheric formaldehyde by wet precipitation, *Environ. Pollut.*, 79, 271–275, doi:10.1016/0269-7491(93)90100-3, 1993.

10 Barkley, M. P., Palmer, P. I., Kuhn, U., Kesselmeier, J., Chance, K., Kurosu, T. P., Martin, R. V., Helmig, D., and Guenther, A.: Net ecosystem fluxes of isoprene over tropical South America inferred from Global Ozone Monitoring Experiment (GOME) observations of HCHO columns, *J. Geophys. Res.*, 113, D20304, doi:10.1029/2008jd009863, 2008.

15 Barkley, M. P., Kurosu, T. P., Chance, K., De Smedt, I., Van Roozendael, M., Arneth, A., Haggberg, D., and Guenther, A.: Assessing sources of uncertainty in formaldehyde air mass factors over tropical South America: implications for top-down isoprene emission estimates, *J. Geophys. Res.-Atmos.*, 117, 1–13, doi:10.1029/2011JD016827, 2012.

Barkley, M. P., De Smedt, I., Van Roozendael, M., Kurosu, T. P., Chance, K., Arneth, A., Haggberg, D., Guenther, A., Paulot, F., Marais, E., and Mao, J.: Top-down isoprene emissions over tropical South America inferred from SCIAMACHY and OMI formaldehyde columns, *J. Geophys. Res.-Atmos.*, 118, 6849–6868, doi:10.1002/jgrd.50552, 2013.

20 Beer, C., Reichstein, M., Tomelleri, E., Ciais, P., Jung, M., Carvalhais, N., Rodenbeck, C., Arain, M. A., Baldocchi, D., Bonan, G. B., Bondeau, A., Cescatti, A., Lasslop, G., Lindroth, A., Lomas, M., Luyssaert, S., Margolis, H., Oleson, K. W., Roupsard, O., Veenendaal, E., Viovy, N., Williams, C., Woodward, F. I., and Papale, D.: Terrestrial gross carbon dioxide uptake: global distribution and covariation with climate, *Science*, 30, 834–838, doi:10.1126/science.1184984, 2010.

25 Beerling, D. J., Nicholas Hewitt, C., Pyle, J. A., and Raven, J. A.: Critical issues in trace gas biogeochemistry and global change, *Philos. Trans. A. Math. Phys. Eng. Sci.*, 365, 1629–1642, doi:10.1098/rsta.2007.2037, 2007.

30 Beerling, D. J., Fox, A., Stevenson, D. S., and Valdes, P. J.: Enhanced chemistry-climate feedbacks in past greenhouse worlds, *Proc. Natl. Acad. Sci. USA*, 108, 9770–9775, doi:10.1073/pnas.1102409108, 2011.

Bonan, G. B., Lawrence, P. J., Oleson, K. W., Levis, S., Jung, M., Reichstein, M., Lawrence, D. M., and Swenson, S. C.: Improving canopy processes in the Community Land

Long-term isoprene variability

Y. Zheng et al.

- Model version 4 (CLM4) using global flux fields empirically inferred from FLUXNET data, *J. Geophys. Res.*, 116, G02014, doi:10.1029/2010jg001593, 2011.
- Carslaw, K. S., Boucher, O., Spracklen, D. V., Mann, G. W., Rae, J. G. L., Woodward, S., and Kulmala, M.: A review of natural aerosol interactions and feedbacks within the Earth system, *Atmos. Chem. Phys.*, 10, 1701–1737, doi:10.5194/acp-10-1701-2010, 2010.
- Ciais, P., Sabine, C., Bala, G., Bopp, L., Borvkin, V., Canadell, J., Chhabra, A., DeFries, R., Gallois, J., Heimann, M., Jones, C., Le Quere, C., Myneni, R. B., Piao, S., and Thornton, P.: Carbon and other biogeochemical cycles, in: Climate Change 2013: The Physical Science Basis. Contribution of Working Group I to the Fifth Assessment Report of the Intergovernmental Panel on Climate Change, Cambridge, UK and New York, NY, USA, 465–570, 2013.
- Collatz, G. J., Ball, J. T., Grivet, C., and Berry, J. A.: Physiological and environmental-regulation of stomatal conductance, photosynthesis and transpiration – a model that includes a laminar boundary-layer, *Agr. Forest Meteorol.*, 54, 107–136, 1991.
- De Smedt, I., Müller, J.-F., Stavrakou, T., van der A, R., Eskes, H., and Van Roozendael, M.: Twelve years of global observations of formaldehyde in the troposphere using GOME and SCIAMACHY sensors, *Atmos. Chem. Phys.*, 8, 4947–4963, doi:10.5194/acp-8-4947-2008, 2008.
- Delwiche, C. F. and Sharkey, T. D.: Rapid appearance of ^{13}C in biogenic isoprene when $^{13}\text{CO}_2$ is fed to intact leaves, *Plant Cell Environ.*, 650, 587–591, doi:10.1111/j.1365-3040.1993.tb00907.x, 1993.
- Farquhar, G. D., Caemmerer, S. V., and Berry, J. A.: A biochemical-model of photosynthetic CO_2 assimilation in leaves of C-3 species, *Planta*, 149, 78–90, 1980.
- Foster, P. N., Prentice, I. C., Morfopoulos, C., Siddall, M., and van Weele, M.: Isoprene emissions track the seasonal cycle of canopy temperature, not primary production: evidence from remote sensing, *Biogeosciences*, 11, 3437–3451, doi:10.5194/bg-11-3437-2014, 2014.
- Friend, A. D. and Kiang, N. Y.: Land surface model development for the GISS GCM: effects of improved canopy physiology on simulated climate, *J. Climate*, 18, 2883–2902, 2005.
- Fu, T.-M., Jacob, D. J., Palmer, P. I., Chance, K., Wang, Y. X., Barletta, B., Blake, D. R., Stanton, J. C., and Pilling, M. J.: Space-based formaldehyde measurements as constraints on volatile organic compound emissions in east and south Asia and implications for ozone, *J. Geophys. Res.*, 112, D06312, doi:10.1029/2006JD007853, 2007.

[Title Page](#)[Abstract](#)[Introduction](#)[Conclusions](#)[References](#)[Tables](#)[Figures](#)[|◀](#)[▶|](#)[◀](#)[▶](#)[Back](#)[Close](#)[Full Screen / Esc](#)[Printer-friendly Version](#)[Interactive Discussion](#)

- González Abad, G., Liu, X., Chance, K., Wang, H., Kurosu, T. P., and Suleiman, R.: Updated Smithsonian Astrophysical Observatory Ozone Monitoring Instrument (SAO OMI) formaldehyde retrieval, *Atmos. Meas. Tech.*, 8, 19–32, doi:10.5194/amt-8-19-2015, 2015.
- 5 Guenther, A. B., Monson, R. K., and Fall, R.: Isoprene and monoterpene emission rate variability: observations with eucalyptus and emission rate algorithm development, *J. Geophys. Res.*, 96, 10799, doi:10.1029/91JD00960, 1991.
- 10 Guenther, A., Hewitt, C. N., Erickson, D., Fall, R., Geron, C., Graedel, T., Harley, P., Klinger, L., Lerdau, M., McKay, W. A., Pierce, T., Scholes, B., Steinbrecher, R., Tallamraju, R., Taylor, J., and Zimmerman, P.: A global-model of natural volatile organic-compound emissions, *J. Geophys. Res.*, 100, 8873–8892, doi:10.1029/94jd02950, 1995.
- Guenther, A., Karl, T., Harley, P., Wiedinmyer, C., Palmer, P. I., and Geron, C.: Estimates of global terrestrial isoprene emissions using MEGAN (Model of Emissions of Gases and Aerosols from Nature), *Atmos. Chem. Phys.*, 6, 3181–3210, doi:10.5194/acp-6-3181-2006, 2006.
- 15 Guenther, A.: Corrigendum to "Estimates of global terrestrial isoprene emissions using MEGAN (Model of Emissions of Gases and Aerosols from Nature)" published in *Atmos. Chem. Phys.*, 6, 3181–3210, 2006, *Atmos. Chem. Phys.*, 7, 4327–4327, doi:10.5194/acp-7-4327-2007, 2007.
- 20 Guenther, A. B., Jiang, X., Heald, C. L., Sakulyanontvittaya, T., Duhl, T., Emmons, L. K., and Wang, X.: The Model of Emissions of Gases and Aerosols from Nature version 2.1 (MEGAN2.1): an extended and updated framework for modeling biogenic emissions, *Geosci. Model Dev.*, 5, 1471–1492, doi:10.5194/gmd-5-1471-2012, 2012.
- 25 Harrison, S. P., Morfopoulos, C., Dani, K. G. S., Prentice, I. C., Arneth, A., Atwell, B. J., Barkley, M. P., Leishman, M. R., Loreto, F., Medlyn, B. E., Niinemets, Ü., Possell, M., Peñuelas, J., and Wright, I. J.: Volatile isoprenoid emissions from plastid to planet, *New Phytol.*, 197, 49–57, doi:10.1111/nph.12021, 2013.
- Heald, C. L. and Spracklen, D. V.: Land use change impacts on air quality and climate, *Chem. Rev.*, doi:10.1021/cr500446g, online first, 2015.
- Hewson, W., Bösch, H., Barkley, M. P., and De Smedt, I.: Characterisation of GOME-2 formaldehyde retrieval sensitivity, *Atmos. Meas. Tech.*, 6, 371–386, doi:10.5194/amt-6-371-2013, 2013.
- 30 Jung, M., Reichstein, M., Margolis, H. A., Cescatti, A., Richardson, A. D., Arain, M. A., Arneth, A., Bernhofer, C., Bonal, D., Chen, J. Q., Gianelle, D., Gobron, N., Kiely, G., Kutsch, W.,

Long-term isoprene variability

Y. Zheng et al.

[Title Page](#)

[Abstract](#)

[Introduction](#)

[Conclusions](#)

[References](#)

[Tables](#)

[Figures](#)

[◀](#)

[▶](#)

[◀](#)

[▶](#)

[Back](#)

[Close](#)

[Full Screen / Esc](#)

[Printer-friendly Version](#)

[Interactive Discussion](#)



Long-term isoprene variability

Y. Zheng et al.

[Title Page](#)

[Abstract](#)

[Introduction](#)

[Conclusions](#)

[References](#)

[Tables](#)

[Figures](#)

[|◀](#)

[▶|](#)

[◀](#)

[▶](#)

[Back](#)

[Close](#)

[Full Screen / Esc](#)

[Printer-friendly Version](#)

[Interactive Discussion](#)



Lasslop, G., Law, B. E., Lindroth, A., Merbold, L., Montagnani, L., Moors, E. J., Papale, D., Sottocornola, M., Vaccari, F., and Williams, C.: Global patterns of land–atmosphere fluxes of carbon dioxide, latent heat, and sensible heat derived from eddy covariance, satellite, and meteorological observations, *J. Geophys. Res.*, 116, G00J07, doi:10.1029/2010jg001566, 2011.

Karl, T., Fall, R., Rosenstiel, T. N., Prazeller, P., Larsen, B., Seufert, G., and Lindinger, W.: Online analysis of the (CO₂)-C-13 labeling of leaf isoprene suggests multiple subcellular origins of isoprene precursors, *Planta*, 215, 894–905, doi:10.1007/S00425-002-0825-2, 2002.

Kirschke, S., Bousquet, P., Ciais, P., Saunois, M., Canadell, J. G., Dlugokencky, E. J., Bergamaschi, P., Bergmann, D., Blake, D. R., Bruhwiler, L., Cameron-Smith, P., Castaldi, S., Chevallier, F., Feng, L., Fraser, A., Heimann, M., Hodson, E. L., Houweling, S., Josse, B., Fraser, P. J., Krummel, P. B., Lamarque, J. F., Langenfelds, R. L., Le Quere, C., Naik, V., O'Doherty, S., Palmer, P. I., Pison, I., Plummer, D., Poulter, B., Prinn, R. G., Rigby, M., Ringeval, B., Santini, M., Schmidt, M., Shindell, D. T., Simpson, I. J., Spahni, R., Steele, L. P., Strode, S. A., Sudo, K., Szopa, S., van der Werf, G. R., Voulgarakis, A., van Weele, M., Weiss, R. F., Williams, J. E., and Zeng, G.: Three decades of global methane sources and sinks, *Nat. Geosci.*, 6, 813–823, doi:10.1038/Ngeo1955, 2013.

Koch, D., Schulz, M., Kinne, S., McNaughton, C., Spackman, J. R., Balkanski, Y., Bauer, S., Berntsen, T., Bond, T. C., Boucher, O., Chin, M., Clarke, A., De Luca, N., Dentener, F., Diehl, T., Dubovik, O., Easter, R., Fahey, D. W., Feichter, J., Fillmore, D., Freitag, S., Ghan, S., Ginoux, P., Gong, S., Horowitz, L., Iversen, T., Kirkevåg, A., Klimont, Z., Kondo, Y., Krol, M., Liu, X., Miller, R., Montanaro, V., Moteki, N., Myhre, G., Penner, J. E., Perlitz, J., Pitari, G., Reddy, S., Sahu, L., Sakamoto, H., Schuster, G., Schwarz, J. P., Seland, Ø., Stier, P., Takegawa, N., Takemura, T., Textor, C., van Aardenne, J. A., and Zhao, Y.: Corrigendum to "Evaluation of black carbon estimations in global aerosol models" published in *Atmos. Chem. Phys.*, 9, 9001–9026, 2009, *Atmos. Chem. Phys.*, 10, 79–81, doi:10.5194/acp-10-79-2010, 2010.

Koster, R. D., Guo, Z. C., Yang, R. Q., Dirmeyer, P. A., Mitchell, K., and Puma, M. J.: On the nature of soil moisture in land surface models, *J. Climate*, 22, 4322–4335, doi:10.1175/2009jcli2832.1, 2009.

Lamarque, J.-F., Bond, T. C., Eyring, V., Granier, C., Heil, A., Klimont, Z., Lee, D., Liousse, C., Mieville, A., Owen, B., Schultz, M. G., Shindell, D., Smith, S. J., Stehfest, E., Van Aardenne, J., Cooper, O. R., Kainuma, M., Mahowald, N., McConnell, J. R., Naik, V., Riahi, K.,

Long-term isoprene variability

Y. Zheng et al.

[Title Page](#)

[Abstract](#)

[Introduction](#)

[Conclusions](#)

[References](#)

[Tables](#)

[Figures](#)

[◀](#)

[▶](#)

[◀](#)

[▶](#)

[Back](#)

[Close](#)

[Full Screen / Esc](#)

[Printer-friendly Version](#)

[Interactive Discussion](#)



and van Vuuren, D. P.: Historical (1850–2000) gridded anthropogenic and biomass burning emissions of reactive gases and aerosols: methodology and application, *Atmos. Chem. Phys.*, 10, 7017–7039, doi:10.5194/acp-10-7017-2010, 2010.

Lathière, J., Hauglustaine, D. A., Friend, A. D., De Noblet-Ducoudré, N., Viovy, N., and Folberth, G. A.: Impact of climate variability and land use changes on global biogenic volatile organic compound emissions, *Atmos. Chem. Phys.*, 6, 2129–2146, doi:10.5194/acp-6-2129-2006, 2006.

Lawrence, P. J. and Chase, T. N.: Representing a new MODIS consistent land surface in the Community Land Model (CLM 3.0), *J. Geophys. Res.*, 112, G01023, doi:10.1029/2006JG000168, 2007.

Marais, E. A., Jacob, D. J., Kurosu, T. P., Chance, K., Murphy, J. G., Reeves, C., Mills, G., Casadio, S., Millet, D. B., Barkley, M. P., Paulot, F., and Mao, J.: Isoprene emissions in Africa inferred from OMI observations of formaldehyde columns, *Atmos. Chem. Phys.*, 12, 6219–6235, doi:10.5194/acp-12-6219-2012, 2012.

Millet, D. B., Jacob, D. J., Boersma, K. F., Fu, T. M., Kurosu, T. P., Chance, K., Heald, C. L., and Guenther, A.: Spatial distribution of isoprene emissions from North America derived from formaldehyde column measurements by the OMI satellite sensor, *J. Geophys. Res.*, 113, D02307, doi:10.1029/2007jd008950, 2008.

Monson, R. K., Trahan, N., Rosenstiel, T. N., Veres, P., Moore, D., Wilkinson, M., Norby, R. J., Volder, A., Tjoelker, M. G., Briske, D. D., Karnosky, D. F., and Fall, R.: Isoprene emission from terrestrial ecosystems in response to global change: minding the gap between models and observations, *Philos. T. R. Soc. A*, 365, 1677–1695, doi:10.1098/Rsta.2007.2038, 2007.

Müller, J.-F., Stavrakou, T., Wallens, S., De Smedt, I., Van Roozendael, M., Potosnak, M. J., Rinne, J., Munger, B., Goldstein, A., and Guenther, A. B.: Global isoprene emissions estimated using MEGAN, ECMWF analyses and a detailed canopy environment model, *Atmos. Chem. Phys.*, 8, 1329–1341, doi:10.5194/acp-8-1329-2008, 2008.

Myhre, G., Samset, B. H., Schulz, M., Balkanski, Y., Bauer, S., Berntsen, T. K., Bian, H., Bellouin, N., Chin, M., Diehl, T., Easter, R. C., Feichter, J., Ghan, S. J., Hauglustaine, D., Iversen, T., Kinne, S., Kirkevåg, A., Lamarque, J.-F., Lin, G., Liu, X., Lund, M. T., Luo, G., Ma, X., van Noije, T., Penner, J. E., Rasch, P. J., Ruiz, A., Selander, Ø., Skeie, R. B., Stier, P., Takemura, T., Tsigaridis, K., Wang, P., Wang, Z., Xu, L., Yu, H., Yu, F., Yoon, J.-H., Zhang, K., Zhang, H., and Zhou, C.: Radiative forcing of the direct aerosol effect from AeroCom Phase II simulations, *Atmos. Chem. Phys.*, 13, 1853–1877, doi:10.5194/acp-13-1853-2013, 2013.

Ninemets, U., Tenhunen, J. D., Harley, P. C., and Steinbrecher, R.: A model of isoprene emission based on energetic requirements for isoprene synthesis and leaf photosynthetic properties for Liquidambar and Quercus, *Plant Cell Environ.*, 22, 1319–1335, 1999.

Pacifico, F., Harrison, S. P., Jones, C. D., Arneth, A., Sitch, S., Weedon, G. P., Barkley, M. P., Palmer, P. I., Serça, D., Potosnak, M., Fu, T.-M., Goldstein, A., Bai, J., and Schurgers, G.: Evaluation of a photosynthesis-based biogenic isoprene emission scheme in JULES and simulation of isoprene emissions under present-day climate conditions, *Atmos. Chem. Phys.*, 11, 4371–4389, doi:10.5194/acp-11-4371-2011, 2011.

Palmer, P. I., Jacob, D. J., Chance, K., Martin, R. V., Spurr, R. J. D., Kurosu, T. P., Bey, I., Yantosca, R., Fiore, A. M., and Li, Q.: Air mass factor formulation for spectroscopic measurements from satellites: application to formaldehyde retrievals from the Global Ozone Monitoring Experiment, *J. Geophys. Res.*, 106, 14539–14550, 2001.

Palmer, P. I., Jacob, D. J., Fiore, A. M., Martin, R. V., Chance, K., and Kurosu, T. P.: Mapping isoprene emissions over North America using formaldehyde column observations from space, 108, 4180, doi:10.1029/2002JD002153, 2003.

Palmer, P. I., Abbot, D. S., Fu, T.-M., Jacob, D. J., Chance, K., Kurosu, T. P., Guenther, A., Wiedinmyer, C., Stanton, J. C., Pilling, M. J., Pressley, S. N., Lamb, B., and Sumner, A. L.: Quantifying the seasonal and interannual variability of North American isoprene emissions using satellite observations of the formaldehyde column, *J. Geophys. Res.*, 111, D12315, doi:10.1029/2005JD006689, 2006.

Porporato, A., Laio, F., Ridolfi, L., and Rodriguez-Iturbe, I.: Plants in water-controlled ecosystems: active role in hydrologic processes and response to water stress – III. Vegetation water stress, *Adv. Water Resour.*, 24, 725–744, doi:10.1016/S0309-1708(01)00006-9, 2001.

Rayner, N. A., Brohan, P., Parker, D. E., Folland, C. K., Kennedy, J. J., Vanicek, M., Ansell, T. J., and Tett, S. F. B.: Improved analyses of changes and uncertainties in sea surface temperature measured in situ since the mid-nineteenth century: the HadSST2 dataset, *J. Climate*, 19, 446–469, 2006.

Rienecker, M. M., Suarez, M. J., Gelaro, R., Todling, R., Bacmeister, J., Liu, E., Bosilovich, M. G., Schubert, S. D., Takacs, L., Kim, G. K., Bloom, S., Chen, J. Y., Collins, D., Conaty, A., Da Silva, A., Gu, W., Joiner, J., Koster, R. D., Lucchesi, R., Molod, A., Owens, T., Pawson, S., Pegion, P., Redder, C. R., Reichle, R., Robertson, F. R., Ruddick, A. G., Sienkiewicz, M., and Woollen, J.: MERRA: NASA's Modern-Era Retrospective Analysis

Title Page

Abstract

Introduction

Conclusions

References

Tables

Figures

|◀

▶|

◀

▶

Back

Close

Full Screen / Esc

Printer-friendly Version

Interactive Discussion



Title Page	
Abstract	Introduction
Conclusions	References
Tables	Figures
◀	▶
◀	▶
Back	Close
Full Screen / Esc	
Printer-friendly Version	
Interactive Discussion	



Schmidt, G. A., Kelley, M., Nazarenko, L., Ruedy, R., Russell, G. L., Aleinov, I., Bauer, M., Bauer, S. E., Bhat, M. K., Bleck, R., Canuto, V., Chen, Y.-H., Cheng, Y., Clune, T. L., Del Genio, A., de Fainchtein, R., Faluvegi, G., Hansen, J. E., Healy, R. J., Kiang, N. Y., Koch, D., Lacis, A. A., LeGrande, A. N., Lerner, J., Lo, K. K., Matthews, E. E., Menon, S., Miller, R. L., Oinas, V., Oloso, A. O., Perlitz, J. P., Puma, M. J., Putman, W. M., Rind, D., Romanou, A., Sato, M., Shindell, D. T., Sun, S., Syed, R. A., Tausnev, N., Tsigaridis, K., Unger, N., Voulgarakis, A., Yao, M.-S., and Zhang, J.: Configuration and assessment of the GISS ModelE2 contributions to the CMIP5 archive, *J. Adv. Model. Earth Syst.*, 6, 141–184, doi:10.1002/2013MS000265, 2014.

Scott, C. E., Rap, A., Spracklen, D. V., Forster, P. M., Carslaw, K. S., Mann, G. W., Pringle, K. J., Kivekäs, N., Kulmala, M., Lihavainen, H., and Tunved, P.: The direct and indirect radiative effects of biogenic secondary organic aerosol, *Atmos. Chem. Phys.*, 14, 447–470, doi:10.5194/acp-14-447-2014, 2014.

Seinfeld, J. H. and Pandis, S. N.: *Atmospheric Chemistry and Physics: From Air Pollution to Climate Change*, 2006.

Shindell, D. T., Lamarque, J.-F., Schulz, M., Flanner, M., Jiao, C., Chin, M., Young, P. J., Lee, Y. H., Rotstyn, L., Mahowald, N., Milly, G., Faluvegi, G., Balkanski, Y., Collins, W. J., Conley, A. J., Dalsoren, S., Easter, R., Ghan, S., Horowitz, L., Liu, X., Myhre, G., Nagashima, T., Naik, V., Rumbold, S. T., Skeie, R., Sudo, K., Szopa, S., Takemura, T., Voulgarakis, A., Yoon, J.-H., and Lo, F.: Radiative forcing in the ACCMIP historical and future climate simulations, *Atmos. Chem. Phys.*, 13, 2939–2974, doi:10.5194/acp-13-2939-2013, 2013a.

Shindell, D. T., Pechony, O., Voulgarakis, A., Faluvegi, G., Nazarenko, L., Lamarque, J.-F., Bowman, K., Milly, G., Kovari, B., Ruedy, R., and Schmidt, G. A.: Interactive ozone and methane chemistry in GISS-E2 historical and future climate simulations, *Atmos. Chem. Phys.*, 13, 2653–2689, doi:10.5194/acp-13-2653-2013, 2013b.

Stevenson, D. S., Young, P. J., Naik, V., Lamarque, J.-F., Shindell, D. T., Voulgarakis, A., Skeie, R. B., Dalsoren, S. B., Myhre, G., Berntsen, T. K., Folberth, G. A., Rumbold, S. T., Collins, W. J., MacKenzie, I. A., Doherty, R. M., Zeng, G., van Noije, T. P. C., Strunk, A., Bergmann, D., Cameron-Smith, P., Plummer, D. A., Strode, S. A., Horowitz, L., Lee, Y. H., Szopa, S., Sudo, K., Nagashima, T., Josse, B., Cionni, I., Righi, M., Eyring, V., Conley, A.,

- Bowman, K. W., Wild, O., and Archibald, A.: Tropospheric ozone changes, radiative forcing and attribution to emissions in the Atmospheric Chemistry and Climate Model Intercomparison Project (ACCMIP), *Atmos. Chem. Phys.*, 13, 3063–3085, doi:10.5194/acp-13-3063-2013, 2013.
- 5 Unger, N.: Human land-use-driven reduction of forest volatiles cools global climate, *Nat. Clim. Chang.*, 4, 907–910, doi:10.1038/nclimate2347, 2014a.
- Unger, N.: On the role of plant volatiles in anthropogenic global climate change, *Geophys. Res. Lett.*, 41, 8563–8569, doi:10.1002/2014GL061616, 2014b.
- 10 Unger, N. and Yue, X.: Strong chemistry-climate feedbacks in the Pliocene, *Geophys. Res. Lett.*, 41, 527–533, doi:10.1002/2013GL058773, 2014.
- 15 Unger, N., Harper, K., Zheng, Y., Kiang, N. Y., Aleinov, I., Arneth, A., Schurgers, G., Ament, C., Goldstein, A., Guenther, A., Heinesch, B., Hewitt, C. N., Karl, T., Laffineur, Q., Langford, B., A. McKinney, K., Misztal, P., Potosnak, M., Rinne, J., Pressley, S., Schoon, N., and Serça, D.: Photosynthesis-dependent isoprene emission from leaf to planet in a global carbon-chemistry-climate model, *Atmos. Chem. Phys.*, 13, 10243–10269, doi:10.5194/acp-13-10243-2013, 2013.
- Von Caemmerer, S. and Farquhar, G. D.: Some relationships between the biochemistry of photosynthesis and the gas-exchange of leaves, *Planta*, 153, 376–387, 1981.
- 20 Wittrock, F., Richter, A., Ladstätter-Weißenmayer, A., and Burrows, J. P.: Global observations of formaldehyde, *Science*, 80, 9–9, 1997.

Long-term isoprene variability

Y. Zheng et al.

[Title Page](#)

[Abstract](#)

[Introduction](#)

[Conclusions](#)

[References](#)

[Tables](#)

[Figures](#)

[|◀](#)

[▶|](#)

[Back](#)

[Close](#)

[Full Screen / Esc](#)

[Printer-friendly Version](#)

[Interactive Discussion](#)



Long-term isoprene variability

Y. Zheng et al.

		Title Page
	Abstract	Introduction
	Conclusions	References
	Tables	Figures
	◀	▶
	◀	▶
	Back	Close
	Full Screen / Esc	
	Printer-friendly Version	
	Interactive Discussion	

Table 1. Regionally averaged meteorological variables with SD from MERRA reanalysis and NASA ModelE2-YIBs in the southeast US and the Amazon.

Southeast US					
		T_s (°C)	PAR (W m^{-2})	SW (W m^{-2})	P (mm day^{-1})
MERRA	MAM	18.0 ± 0.8	110.1 ± 3.4	250.0 ± 8.3	2.6 ± 0.7
	JJA	26.8 ± 0.5	108.5 ± 3.7	237.8 ± 9.0	4.8 ± 0.5
	SON	18.6 ± 0.8	80.7 ± 4.3	182.3 ± 10.5	2.8 ± 0.7
ModelE2-YIBs	MAM	18.6 ± 0.8	106.8 ± 2.3	237.4 ± 5.0	4.2 ± 0.5
	JJA	26.8 ± 0.4	118.7 ± 1.5	263.7 ± 3.4	4.5 ± 0.6
	SON	20.5 ± 1.3	82.1 ± 1.9	182.4 ± 4.2	2.3 ± 0.7
Amazon					
MERRA	MAM	23.5 ± 0.5	89.9 ± 2.7	193.4 ± 6.0	7.9 ± 0.4
	JJA	23.7 ± 0.4	99.4 ± 3.1	219.9 ± 7.6	3.5 ± 0.5
	SON	25.3 ± 0.6	103.3 ± 4.2	226.0 ± 9.7	4.9 ± 0.6
ModelE2-YIBs	MAM	26.4 ± 0.2	100.3 ± 0.8	222.8 ± 1.7	6.0 ± 0.3
	JJA	26.4 ± 0.3	94.0 ± 0.9	208.9 ± 2.1	2.2 ± 0.2
	SON	28.6 ± 0.4	102.6 ± 1.0	228.1 ± 2.1	3.3 ± 0.3



[Title Page](#)[Abstract](#)[Introduction](#)[Conclusions](#)[References](#)[Tables](#)[Figures](#)[|◀](#)[▶|](#)[◀](#)[▶](#)[Back](#)[Close](#)[Full Screen / Esc](#)[Printer-friendly Version](#)[Interactive Discussion](#)

Table 2. Regionally averaged MLR β -coefficients with SD for GPP and HCHOv in the southeast US, defined as (31 to 35° N; –94 to –79° E) and the Amazon defined as (–15° S to 3° N, –76° to –54° E). The covariance of GPP with T_s , PAR and precipitation (P) are denoted as GPP_β_ T_s , GPP_β_PAR, GPP_β_ P ; the covariance of HCHOv with T_s , SW and precipitation (P) are denoted as HCHOv_β_ T_s , HCHOv_β_SW, HCHOv_β_ P . In MLR of OMI-HCHOv (a), (b) and (c), the OMI-HCHO columns are processed using model Y-PS, Y-MEGAN and Y-MEGAN-SM, respectively.

Southeast US			
MLR of FLUXNET-GPP: 1982–2011			
	GPP_β_ T_s	GPP_β_PAR	GPP_β_ P
MAM	0.58 ± 0.11	0.44 ± 0.10	0.19 ± 0.05
JJA	0.03 ± 0.25	0.41 ± 0.52	0.35 ± 0.30
SON	0.41 ± 0.13	0.51 ± 0.10	0.18 ± 0.08
MLR of OMI-HCHOv: 2005–2013			
	HCHOv_β_ T_s	HCHOv_β_SW	HCHOv_β_ P
MAM	(a) 0.36 ± 0.34 (b) 0.36 ± 0.33 (c) 0.36 ± 0.33	(a) –0.02 ± 0.32 (b) –0.02 ± 0.31 (c) –0.02 ± 0.31	(a) 0.05 ± 0.35 (b) 0.05 ± 0.35 (c) 0.04 ± 0.35
JJA	(a) 0.31 ± 0.22 (b) 0.31 ± 0.22 (c) 0.31 ± 0.22	(a) 0.16 ± 0.38 (b) 0.17 ± 0.38 (c) 0.17 ± 0.38	(a) 0.26 ± 0.51 (b) 0.26 ± 0.51 (c) 0.26 ± 0.51
SON	(a) 0.53 ± 0.77 (b) 0.51 ± 0.77 (c) 0.52 ± 0.77	(a) –0.18 ± 0.67 (b) –0.16 ± 0.66 (c) –0.17 ± 0.66	(a) –0.02 ± 0.37 (b) –0.01 ± 0.37 (c) –0.01 ± 0.37

Table 2. Continued.

Amazon			
MLR of FLUXNET-GPP: 1982–2011			
	GPP_β_T _s	GPP_β_PAR	GPP_β_P
MAM	0.11 ± 0.17	0.46 ± 0.32	0.70 ± 0.40
JJA	0.14 ± 0.20	0.57 ± 0.54	0.27 ± 0.39
SON	0.24 ± 0.19	0.17 ± 0.50	0.50 ± 0.53
MLR of OMI-HCHOv: 2005–2013			
	HCHOv_β_T _s	HCHOv_β_SW	HCHOv_β_P
MAM	(a) 0.16 ± 0.27 (b) 0.16 ± 0.27 (c) 0.16 ± 0.27	(a) 0.00 ± 0.27 (b) 0.00 ± 0.27 (c) 0.00 ± 0.27	(a) -0.04 ± 0.29 (b) -0.05 ± 0.29 (c) -0.05 ± 0.29
JJA	(a) 0.18 ± 0.33 (b) 0.18 ± 0.33 (c) 0.18 ± 0.33	(a) 0.31 ± 0.54 (b) 0.31 ± 0.54 (c) 0.31 ± 0.53	(a) 0.03 ± 0.47 (b) 0.03 ± 0.47 (c) 0.03 ± 0.47
SON	(a) 0.03 ± 0.46 (b) 0.04 ± 0.46 (c) 0.03 ± 0.46	(a) 0.01 ± 0.52 (b) 0.01 ± 0.52 (c) 0.01 ± 0.52	(a) -0.31 ± 0.56 (b) -0.31 ± 0.56 (c) -0.31 ± 0.56

Long-term isoprene variability

Y. Zheng et al.

[Title Page](#)[Abstract](#)[Introduction](#)[Conclusions](#)[References](#)[Tables](#)[Figures](#)[◀](#)[▶](#)[Back](#)[Close](#)[Full Screen / Esc](#)[Printer-friendly Version](#)[Interactive Discussion](#)

Long-term isoprene variability

Y. Zheng et al.

[Title Page](#)

[Abstract](#)

[Introduction](#)

[Conclusions](#)

[References](#)

[Tables](#)

[Figures](#)

[|◀](#)

[▶|](#)

[◀](#)

[▶](#)

[Back](#)

[Close](#)

[Full Screen / Esc](#)

[Printer-friendly Version](#)

[Interactive Discussion](#)



Table 3. Summary of regionally averaged observational and simulated seasonal correlation coefficients in the southeast US and the Amazon. In observational GPP-HCHOv (a), (b) and (c), the OMI-HCHO columns are processed using model Y-PS, Y-MEGAN and Y-MEGAN-SM, respectively.

		Southeast US		
		GPP-HCHOv	GPP-ISOPe	ISOPe-HCHOv
Observation	MAM	(a) 0.24 ± 0.10	–	–
		(b) 0.24 ± 0.10	–	–
		(c) 0.24 ± 0.10	–	–
	JJA	(a) -0.03 ± 0.10	–	–
		(b) -0.03 ± 0.11	–	–
		(c) -0.03 ± 0.10	–	–
	SON	(a) 0.25 ± 0.10	–	–
		(b) 0.26 ± 0.10	–	–
		(c) 0.26 ± 0.10	–	–
Y-PS	MAM	0.86 ± 0.16	0.98 ± 0.01	0.88 ± 0.14
	JJA	-0.19 ± 0.30	0.94 ± 0.07	-0.03 ± 0.31
	SON	0.68 ± 0.22	0.97 ± 0.01	0.71 ± 0.20
Y-MEGAN	MAM	0.77 ± 0.22	0.86 ± 0.14	0.97 ± 0.02
	JJA	-0.62 ± 0.19	-0.39 ± 0.23	0.73 ± 0.09
	SON	0.52 ± 0.26	0.69 ± 0.17	0.94 ± 0.05
Y-MEGAN-SM	MAM	0.81 ± 0.19	0.95 ± 0.02	0.91 ± 0.11
	JJA	-0.37 ± 0.22	0.79 ± 0.19	0.08 ± 0.35
	SON	0.61 ± 0.23	0.92 ± 0.02	0.80 ± 0.16

Long-term isoprene variability

Y. Zheng et al.

		Amazon		
		GPP-HCHOv	GPP-ISOPe	ISOPe-HCHOv
Observation	MAM	(a) 0.11 ± 0.19	–	–
		(b) 0.11 ± 0.20	–	–
		(c) 0.11 ± 0.20	–	–
	JJA	(a) 0.33 ± 0.30	–	–
		(b) 0.33 ± 0.30	–	–
		(c) 0.33 ± 0.30	–	–
	SON	(a) -0.09 ± 0.20	–	–
		(b) -0.09 ± 0.20	–	–
		(c) -0.09 ± 0.20	–	–
Y-PS	MAM	0.34 ± 0.35	0.79 ± 0.25	0.36 ± 0.31
	JJA	0.05 ± 0.46	0.84 ± 0.84	0.10 ± 0.49
	SON	-0.14 ± 0.49	0.87 ± 0.87	-0.11 ± 0.44
Y-MEGAN	MAM	0.02 ± 0.49	0.07 ± 0.54	0.31 ± 0.31
	JJA	-0.08 ± 0.51	-0.03 ± 0.62	0.62 ± 0.29
	SON	-0.51 ± 0.41	-0.46 ± 0.51	0.49 ± 0.31
Y-MEGAN-SM	MAM	0.10 ± 0.45	0.52 ± 0.42	0.14 ± 0.40
	JJA	-0.01 ± 0.49	0.45 ± 0.37	0.17 ± 0.42
	SON	-0.39 ± 0.42	0.49 ± 0.44	-0.13 ± 0.49

- [Title Page](#)
- [Abstract](#) [Introduction](#)
- [Conclusions](#) [References](#)
- [Tables](#) [Figures](#)
- [◀](#) [▶](#)
- [◀](#) [▶](#)
- [Back](#) [Close](#)
- [Full Screen / Esc](#)
- [Printer-friendly Version](#)
- [Interactive Discussion](#)



Long-term isoprene variability

Y. Zheng et al.

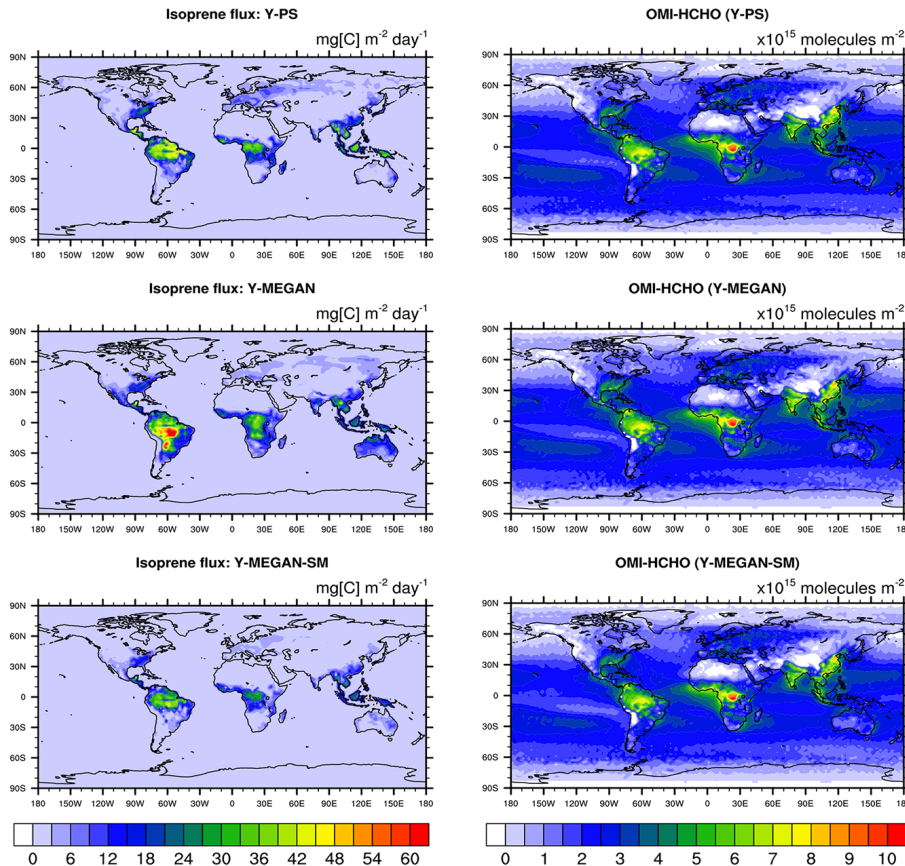


Figure 1. Left column: simulated annual mean isoprene flux ($\text{mg C m}^{-2} \text{ day}^{-1}$) in model Y-PS, Y-MEGAN and Y-MEGAN-SM. Right column: satellite-based HCHO columns ($\times 10^{15} \text{ molecules m}^{-2}$) from OMI processed using air-mass-factors from model Y-PS, Y-MEGAN and Y-MEGAN-SM.

[Title Page](#)[Abstract](#)[Introduction](#)[Conclusions](#)[References](#)[Tables](#)[Figures](#)[|◀](#)[▶|](#)[◀](#)[▶|](#)[Back](#)[Close](#)[Full Screen / Esc](#)[Printer-friendly Version](#)[Interactive Discussion](#)

Long-term isoprene variability

Y. Zheng et al.

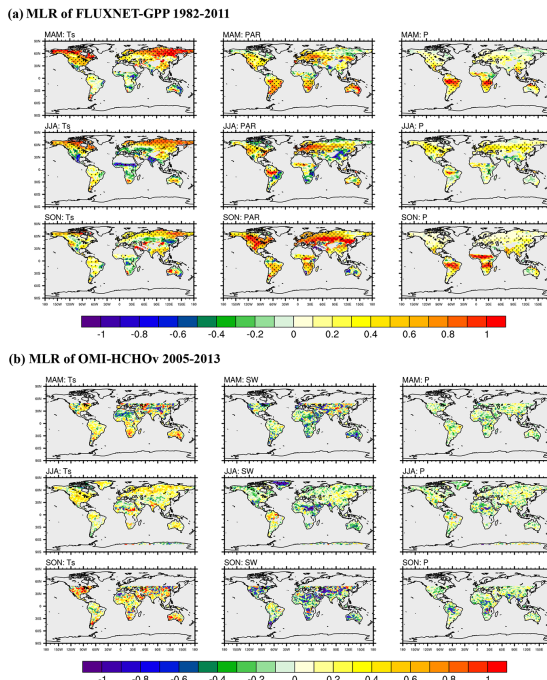


Figure 2. (a) The covariance of FLUXNET-GPP with monthly mean surface temperature (T_s), photosynthetically active radiation (PAR) and precipitation (P) in MAM (top), JJA (middle) and SON (bottom) from the MLR analysis. MLR is calculated using monthly mean data in 1982–2011. Significant regions ($p < 0.05$) are shown with dotted shading. (b) The covariance of OMI-HCHOv with monthly mean surface temperature (T_s), downward shortwave radiation (SW) and precipitation (P) in MAM (top), JJA (middle) and SON (bottom) from the MLR analysis. MLR is calculated using monthly mean data in 2005–2013. Significant regions ($p < 0.05$) are shown with dotted shading.

[Title Page](#)

[Abstract](#)

[Introduction](#)

[Conclusions](#)

[References](#)

[Tables](#)

[Figures](#)

◀

▶

◀

▶

[Back](#)

[Close](#)

[Full Screen / Esc](#)

[Printer-friendly Version](#)

[Interactive Discussion](#)



Long-term isoprene variability

Y. Zheng et al.

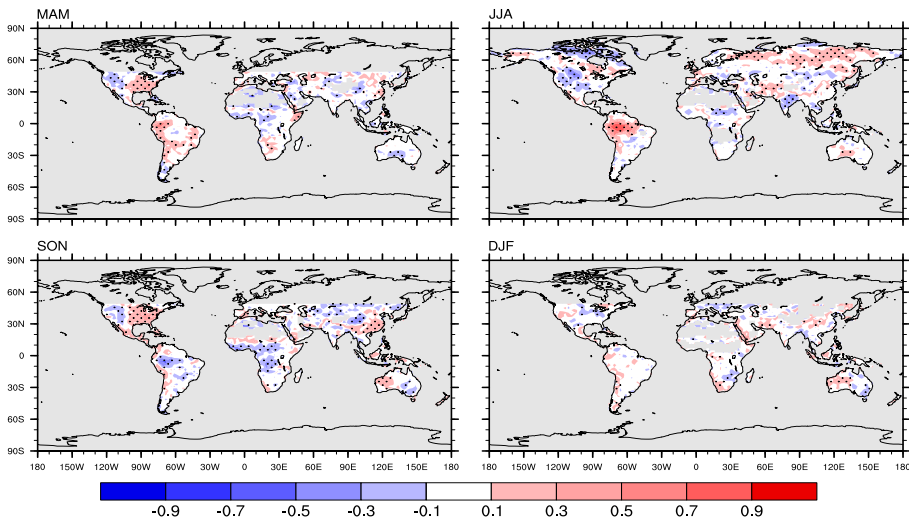


Figure 3. Observed correlation between monthly mean FLUXNET-GPP and OMI-HCHOv in four seasons: MAM, JJA, SON and DJF. Significant regions ($p < 0.05$) are shown with dotted shading.

[Title Page](#)[Abstract](#)[Introduction](#)[Conclusions](#)[References](#)[Tables](#)[Figures](#)[Back](#)[Close](#)[Full Screen / Esc](#)[Printer-friendly Version](#)[Interactive Discussion](#)

Discussion Paper | Long-term isoprene variability

Y. Zheng et al.

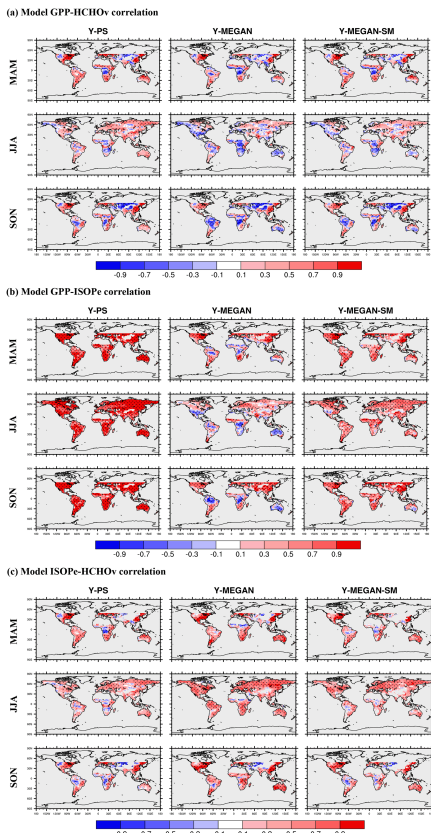


Figure 4. Simulated correlation between monthly mean **(a)** GPP and HCHOv, **(b)** GPP and ISOPE, **(c)** ISOPE and HCHOv in MAM, JJA and SON using three isoprene algorithms: Y-PS, Y-MEGAN, Y-MEGAN-SM. Significant regions ($p < 0.05$) are shown with dotted shading.